

# Diffraction enhanced transparency in a hybrid gold-graphene THz metasurface

**Citation for published version (APA):**

van Hoof, N. J. J., ter Huurne, S. E. T., Vervuurt, R. H. J., Bol, A. A., Halpin, A., & Rivas, J. G. (2019). Diffraction enhanced transparency in a hybrid gold-graphene THz metasurface. *APL Photonics*, 4(3), Article 036104. <https://doi.org/10.1063/1.5080390>

**Document license:**  
CC BY

**DOI:**  
[10.1063/1.5080390](https://doi.org/10.1063/1.5080390)

**Document status and date:**  
Published: 01/03/2019

**Document Version:**  
Publisher's PDF, also known as Version of Record (includes final page, issue and volume numbers)

**Please check the document version of this publication:**

- A submitted manuscript is the version of the article upon submission and before peer-review. There can be important differences between the submitted version and the official published version of record. People interested in the research are advised to contact the author for the final version of the publication, or visit the DOI to the publisher's website.
- The final author version and the galley proof are versions of the publication after peer review.
- The final published version features the final layout of the paper including the volume, issue and page numbers.

[Link to publication](#)

**General rights**

Copyright and moral rights for the publications made accessible in the public portal are retained by the authors and/or other copyright owners and it is a condition of accessing publications that users recognise and abide by the legal requirements associated with these rights.

- Users may download and print one copy of any publication from the public portal for the purpose of private study or research.
- You may not further distribute the material or use it for any profit-making activity or commercial gain
- You may freely distribute the URL identifying the publication in the public portal.

If the publication is distributed under the terms of Article 25fa of the Dutch Copyright Act, indicated by the "Taverne" license above, please follow below link for the End User Agreement:

[www.tue.nl/taverne](http://www.tue.nl/taverne)

**Take down policy**

If you believe that this document breaches copyright please contact us at:






[openaccess@tue.nl](mailto:openaccess@tue.nl)

providing details and we will investigate your claim.

# Diffraction enhanced transparency in a hybrid gold-graphene THz metasurface

Cite as: APL Photonics 4, 036104 (2019); <https://doi.org/10.1063/1.5080390>

Submitted: 08 November 2018 . Accepted: 04 March 2019 . Published Online: 27 March 2019

Niels J. J. van Hoof , Stan E. T. ter Huurne, René H. J. Vervuurt , Ageeth A. Bol , Alexei Halpin , and Jaime Gómez Rivas 



View Online



Export Citation



CrossMark

## ARTICLES YOU MAY BE INTERESTED IN

[Enhanced on-chip terahertz sensing with hybrid metasurface/lithium niobate structures](#)

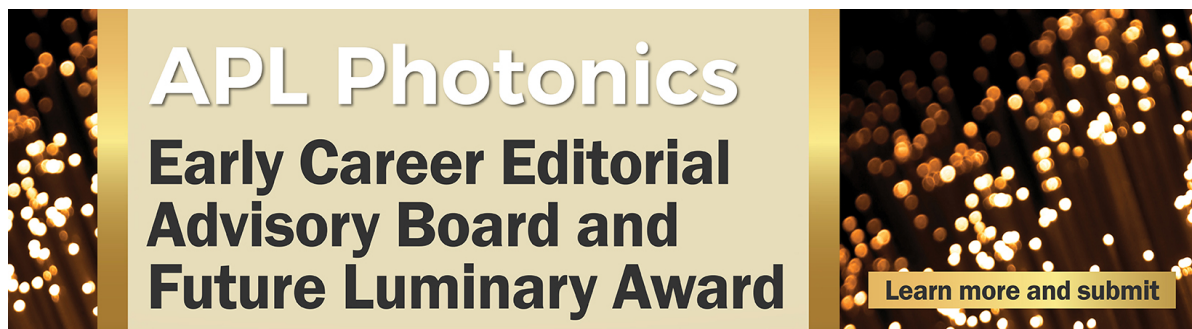
Applied Physics Letters **114**, 121102 (2019); <https://doi.org/10.1063/1.5087609>

[Optimized nonlinear terahertz response of graphene in a parallel-plate waveguide](#)

APL Photonics **4**, 034401 (2019); <https://doi.org/10.1063/1.5045652>

[Nonlinear plasmonics of three-dimensional Dirac semimetals](#)

APL Photonics **4**, 034402 (2019); <https://doi.org/10.1063/1.5042450>



**APL Photonics**  
**Early Career Editorial  
Advisory Board and  
Future Luminary Award**

[Learn more and submit](#)

# Diffraction enhanced transparency in a hybrid gold-graphene THz metasurface

Cite as: APL Photon. 4, 036104 (2019); doi: 10.1063/1.5080390

Submitted: 8 November 2018 • Accepted: 4 March 2019 •

Published Online: 27 March 2019



Niels J. J. van Hoof,<sup>1,2,a)</sup> Stan E. T. ter Huurne,<sup>1,a)</sup> René H. J. Vervuurt,<sup>1</sup> Ageeth A. Bol,<sup>1</sup> Alexei Halpin,<sup>2</sup> and Jaime Gómez Rivas<sup>1</sup>

## AFFILIATIONS

<sup>1</sup>Department of Applied Physics, Institute for Photonic Integration, Eindhoven University of Technology, P.O. Box 513, 5600 MB Eindhoven, The Netherlands

<sup>2</sup>Dutch Institute for Fundamental Energy Research-DIFFER, De Zaaie 20, 5612AJ Eindhoven, The Netherlands

<sup>a)</sup>**Contributions:** N. J. J. van Hoof and S. E. T. ter Huurne contributed equally to this work.

## ABSTRACT

Terahertz (THz) near-field microscopy is used to investigate the underlying physics that leads to diffraction enhanced transparency (DET) in a periodic array of detuned metallic rods. At the transparency frequency, the system is highly dispersive and THz radiation is delayed for several tens of picoseconds before being re-emitted into the forward direction. Using polarization sensitive measurements of the electric THz near-field spectrum, we demonstrate that an out-of-phase field distribution is formed in the unit cell leading to a reduced coupling to the far-field. This quadrupolar field distribution originates from the excitation and interference of surface lattice modes produced by the enhanced radiative coupling through the lattice of localized resonances in the metallic rods. These results represent the first experimental near-field investigation of DET, shedding light onto this phenomenon and providing important information for its further development. Implementing DET in applications requires control over the transparency window. We demonstrate that adding a monolayer of graphene, absorbing at THz frequencies, is sufficient to fully suppress the DET despite its monoatomic thickness. This efficient suppression is due to the diffractive wave character of DET and a metal insulator metal resonance formed between the localized resonance of the gold resonator and the extended graphene layer. The possibility to exert control over the transparency window by changing the conductivity of graphene by altering the Fermi level opens the possibility of active THz devices.

© 2019 Author(s). All article content, except where otherwise noted, is licensed under a Creative Commons Attribution (CC BY) license (<http://creativecommons.org/licenses/by/4.0/>). <https://doi.org/10.1063/1.5080390>

## I. INTRODUCTION

The large scattering cross sections of conducting resonant structures leads to field localization<sup>1,2</sup> and can be exploited to manipulate electromagnetic radiation. Designed arrangements of these structures on a surface leads to scattering and interference that enables wavefront shaping.<sup>3</sup> Active control of near-fields and wavefronts has fueled the research field of metasurfaces, opening interesting perspectives for applications at terahertz (THz) frequencies.<sup>4-7</sup> One of the most interesting phenomena that has been reported with resonant scatterers on structured surfaces is analogous to electromagnetically induced transparency (EIT).<sup>8</sup> EIT refers to the quantum interference of two optical fields interacting with quantum states in an absorbing material. Within the so-called “transparency window,” this interference will render the material

transparent, while still being at resonance with the incident light field.<sup>9</sup> The interest in EIT resides in the strong dispersion in the transparency window that will significantly delay the wave propagation,<sup>10</sup> finding applications in THz communication and sensing.<sup>11,12</sup> The recent analogy of EIT with a classical model of coupled oscillators has sparked a large interest in the realization of this phenomenon in resonant systems across the electromagnetic spectrum.<sup>13-15</sup> One of the most severe limitations of EIT in a set of coupled oscillators is the requirement of efficient coupling, which has limited most of the studies to near-field coupling.<sup>8,16-18</sup> However, near-field coupling requires the resonators to be positioned with a spatial precision much smaller than the wavelength of radiation, which limits the tolerance in the fabrication and the realization of EIT metasurfaces. Therefore, the recent suggestion that radiative coupling of detuned resonators can lead to EIT,<sup>19,20</sup> and

the demonstration that this effect can be significantly improved by exploiting the radiation enhanced coupling through in-plane diffraction, will enable new designs of metasurfaces with improved performance.<sup>21-23</sup> However, for applications such as high data rate communication, sensing, and non-linear optics, one still needs active control over the frequency response, which can be acquired when combining a static EIT surface, built on quartz and resonant conducting structures, with a tunable material system.

The unique properties of two-dimensional (2D) materials, such as high electron mobility and electrical tunability of graphene, have driven the scientific community to produce and investigate these materials eagerly.<sup>24,25</sup> Free electrons in graphene follow a Drude-like behavior with significant absorption at THz frequencies even though it consists of only a single atomic layer.<sup>26,27</sup> The linear electronic band diagram of graphene enables the continuous tuning of the carrier density, that consequently, alters the response of graphene to THz radiation. Many promising metasurfaces solely based on patterned graphene have been predicted.<sup>28-30</sup> However, experimental realization has proven difficult as the quality of graphene has to be exceptional.<sup>31,32</sup> Therefore, the resonant response of graphene based structures at THz frequencies is currently achieved in hybrid structures in which graphene is combined with metallic resonators and metasurfaces. With these combinations, it is possible to exploit the tunability of the response of graphene with the large scattering cross sections of resonant metallic structures.<sup>32-38</sup>

In this manuscript, we demonstrate a metal-graphene hybrid metasurface with a tunable transparency window at THz frequencies consisting of a periodic pattern of gold particles. When a single gold particle of appropriately chosen dimensions is aligned with the polarization of THz radiation, it will exhibit a (dipolar-like)  $\lambda/2$  resonance. These localized resonances are spectrally broad, but can be enhanced by arranging the resonators in an array. Diffraction in the plane of the array through the so-called Rayleigh Anomalies (RAs) leads to an enhanced radiative coupling of localized resonances when they are frequency matched.<sup>39-41</sup> These resonances are called surface lattice resonances (SLRs) and have sharp spectral features in the vicinity of the RA. The metasurface described in this manuscript is designed to exhibit a transparency window arising from the interference of two SLRs,<sup>23</sup> and this phenomenon is known as lattice- or diffraction-enhanced transparency (DET). DET does not rely on near-field coupling of nearby resonators but is achieved by creating an array with two frequency detuned resonators per unit cell. The resonators are spread out symmetrically such that the distance to the next neighbor is half of the unit cell size. The different resonance frequencies are achieved by varying the lengths of the resonators. As we will show, the coupling and interference between SLRs leads to a frequency window in which the transmittance approaches unity, while the electric field close to the resonators is enhanced significantly. To unravel the underlying dynamics of DET, we have measured the associated THz electric near-field amplitude and phase. These measurements show how the two SLRs couple to form an out-of-phase field distribution that suppresses the coupling to far-field radiation at the resonant frequency and results in a sharp transparency window. Bringing a monolayer of graphene in close proximity to the array reduces the field enhancement around the resonant structures by an order of magnitude and fully suppresses DET. This remarkable response is caused by the

surface character of the SLRs and by the confinement of the THz field between graphene and gold particles, which forms a metal-insulator-metal (MIM) structure. Furthermore, changing the Fermi level of graphene by ambient doping modifies the THz field distribution around the detuned resonators, which enables the tuning of DET.

## II. RESULTS

### A. Sample fabrication

The array was fabricated using optical lithography, metal deposition, and lift-off techniques. It consists of a  $2 \times 2$  cm<sup>2</sup> 2D square lattice of gold rods with a lattice constant of 300  $\mu\text{m}$ . The particles in the unit cell are formed by two 100 nm thick gold rods with different lateral dimensions. The “long” rod has a length and a width of 200  $\mu\text{m}$  and 40  $\mu\text{m}$ , respectively; while the “short” rod is 125  $\mu\text{m}$  long and 60  $\mu\text{m}$  wide. The difference in length of the two rods will lead to different natural frequencies when illuminated with polarized THz radiation along their long axes. The widths of the two types of rods are different to ensure that the volume and surface coverage are the same, making their off-resonance polarizability in first approximation similar. The  $\lambda/2$  resonances of the long and short resonators are designed to be frequency detuned and resonant at approximately 0.4 and 0.5 THz, respectively, when deposited on a medium of refractive index 2.1 (i.e., quartz). The center-to-center distance between rods is 150  $\mu\text{m}$ , making the array highly symmetrical. This sample design was based on a previous study.<sup>23</sup>

For our experiments, graphene has been grown using chemical vapor deposition (CVD)<sup>42</sup> and transferred onto the array of detuned resonators with a 300 nm thick PMMA substrate.<sup>43</sup> The transfer is carried out such that the PMMA is located between the gold rods and the graphene, acting as an insulating layer. The layer of PMMA on its own has no significant effect on the THz transmission. A dark-field optical microscope image of the sample is shown in Fig. 1.

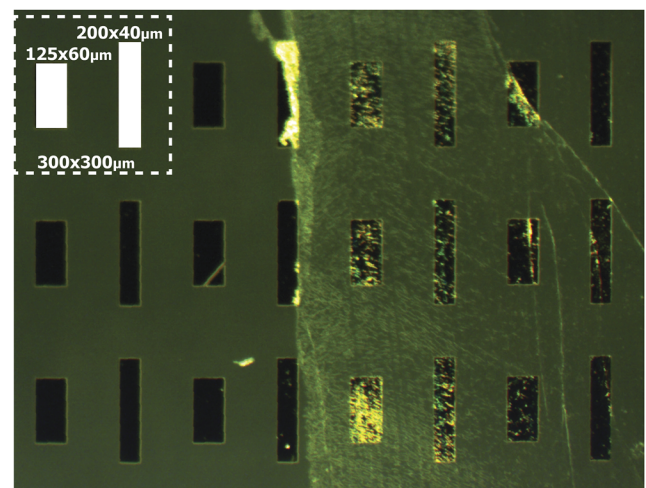


**FIG. 1.** Dark-field microscope image of an array of detuned resonators of which the right half is covered by a monolayer of graphene. A single unit cell is graphically illustrated and labeled with dimensions.

This image shows the edge between the bare (left) and graphene covered (right) part of the array. The edge between the covered and uncovered parts of the sample is defined by the transfer process and was created on purpose to enable reference measurements with and without graphene on the same sample. The PMMA layer with the graphene monolayer on top shows a high density of cracks close to the edges, as can be appreciated by the turbid image in Fig. 1. This optical contrast is caused by the thicker PMMA at the edges leading to the formation of these cracks. Further away from the edge, the image is more clear and the graphene is uniform, showing no signs of cracks. The measurements shown in this manuscript have been obtained at least 15 unit cells away from the graphene edges.

## B. Far-field transmittance

The far-field transmittance spectra of the samples were measured with a THz time-domain spectrometer that records the THz transient as it passes through the sample and is Fourier transformed to get transmission spectra. The setup consists of a photoconductive antenna and a photoconductive switch separated by lenses in a 4- $f$  configuration (see the inset of Fig. 2). The polarization of the incident THz radiation is oriented along the long axis of the resonators (vertical in Fig. 1). These measurements are shown in Fig. 2 for the bare (blue curve) and graphene covered (red curve) arrays of detuned resonators. The far-field measurements are referenced to a quartz substrate to obtain the transmittance.

The bare array shows a minimum in transmittance at 0.4 THz, followed by a peak in transmittance at 0.45 THz, after which the transmission drops again at 0.5 THz. At 0.4 THz, the transmittance vanishes because predominantly the long rods are resonant with the incident THz field, as will be illustrated later by near-field measurements. At this frequency, the radiation is efficiently scattered by the long rods into the array, exciting a SLR. Similarly, at 0.5 THz, the short rods are predominately resonant with the incident radiation, thus exciting a SLR through the short rods. At 0.45 THz, both long and short rods react to the incident field but are out-of-phase, creating a mode that is weakly coupled to the far field resulting

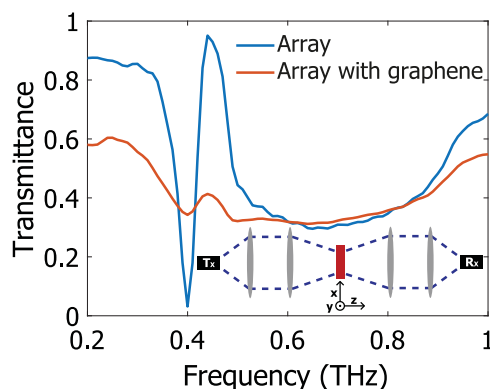


**FIG. 2.** Far-field THz transmittance spectra of the bare (blue curve) and graphene covered (red curve) array of detuned resonators, normalized to the THz transmission through a quartz substrate. The inset schematically shows a top-down view of the 4- $f$  THz-TDS setup that was used, where Tx is the transmitter and Rx is the receiver.

in a high transmittance. This transmission spectrum, with a sharp and pronounced transparency window at 0.45 THz, in which the transmission reaches almost unity, is produced by the interference between these two SLRs, generated by the short and long rods coupling to each other through the in-plane diffraction supported by the array.<sup>23</sup> Transmission through the constituent parts of the array are included in the [supplementary material](#), as shown in Fig. SI.1. It is important to stress that the transparency window at 0.45 THz is generated while the structure is still resonant with the incident field; therefore, this phenomenon is known as diffraction enhanced transparency (DET). DET induces a significant group delay as the THz wave at this frequency is scattered in the plane of the array before coupling out into the forward direction.<sup>23,44</sup>

A monolayer of CVD grown graphene on its own shows a strong response to THz radiation, reducing the transmitted intensity by  $\sim 30\%$ .<sup>45</sup> We can leverage the scattering properties of the array by placing graphene on top of the array of detuned resonators. The THz field of SLRs will have a significant spatial overlap with graphene as both the surface modes and the graphene monolayer extend over the plane of the array. The measured transmittance spectrum of the graphene covered array is shown in Fig. SI.2 (red curve). The minimum of transmittance at 0.4 THz is increased sixfold, while the transmittance at the DET window is reduced by 50%. These changes are larger than the incoherent sum of the graphene and array measured separately and thus infers the coupling of graphene with the surface lattice resonances forming hybrid gold-graphene THz metasurface; see Fig. SI.2 in the [supplementary material](#). We will further evaluate the sample using near-field microscopy at three different frequencies, namely, 0.4, 0.45, and 0.5 THz, to identify the coupling of SLRs in the formation of DET and to show how SLRs and DET are affected by graphene.

## C. Near-field microscopy

Studying the interaction of THz radiation with sub-diffraction structures requires near-field measurements. The THz near-field microscope used for our measurements has been described previously,<sup>46,47</sup> where THz microprobes (Protemics GmbH) are used to detect the polarization dependent electric near-field at a distance of  $0.5 \mu\text{m}$  above the sample. The spatially and temporally resolved near-fields are collected by raster scanning the sample through the optical axis defined by the incident THz beam and the near-field microprobe. Fourier analysis of the measured THz transients allows for the generation of 2D spectral maps. Spatially dependent polarization sensitive measurements carry information about the near-field enhancement in proximity of the resonators. By measuring both the out-of-plane ( $E_z$ ) and cross-polarized ( $E_x$ ) components of the electric field with respect to the polarized illumination along the  $y$ -direction, we obtain information about the local field enhancements and visualize the diffractive nature of the SLRs.

Before presenting the full 2D spectral maps, we first discuss a single transient. Figure 3 shows the  $E_z$  component of the electric field at the edge of a long rod, both on the bare (blue curve) and graphene covered (red curve) array of detuned resonators. We observe that the electric field on the bare array oscillates for more than 25 ps, while the oscillations in the graphene covered array are quenched within 7 ps. The first field oscillation through the graphene covered array (centered at  $t = 0$ ) has a reduction in an amplitude of



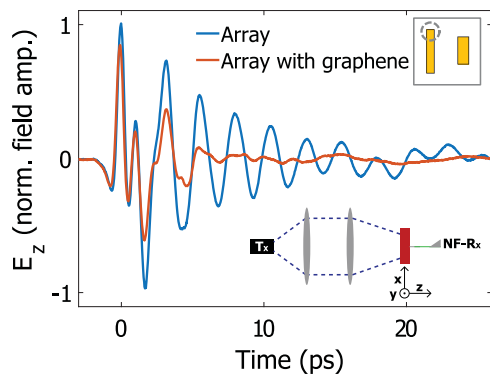


**FIG. 3.** Out-of-plane electric near-field component ( $E_z$ ) measured at the edge of a long rod as a function of time. The blue curve corresponds to the bare array of detuned resonators and the red curve to the same array covered by graphene. The inset schematically shows a top-down view of the near-field THz-TDS setup that was used, where Tx is the transmitter and NF-Rx is the near-field receiver.

16%, in agreement with the direct absorption by the graphene layer. However, consecutive field oscillations get attenuated more severely as the THz field would normally be diffracted into the plane and propagate along the surface, but this is inhibited by the presence of graphene. This reduction makes the system more interesting as the monolayer of graphene acts on both the incident and scattered THz fields. We can create 2D spectral maps for independently measured polarizations, by Fourier transforming the spatially resolved transients, such as the one shown in Fig. 3, these will be discussed next.

The 2D spectral maps of the out-of-plane electric near-field amplitude ( $E_z$ ) have been plotted for the three frequencies of interest discussed before, i.e., 0.4, 0.45, and 0.5 THz. These measurements are shown across a single unit cell in Figs. 4(a)–4(c), respectively, where

the THz amplitude maps are normalized to the maximum near-field amplitudes obtained at 0.45 THz. The electric near-field is localized on the long rod at 0.4 THz [Fig. 4(a)], and it is in-phase with the applied electric field. The short rod shows no significant enhancement as its fundamental resonance lies at a higher frequency. At 0.5 THz, the response of the long and short rods is reversed, as can be seen in Fig. 4(c) where the near-field localization is mainly on the short rod. However, the long rod exhibits a near-field enhancement as well, as it has a finite polarizability at this frequency.

Figure 4(b) shows the electric near-field at the frequency of the diffraction enhanced transparency. Both rods display a large field enhancement while being opposite in the phase. The near-field close to the long rod has reversed its polarity with respect to the incident THz field. As 0.45 THz is above the natural frequency of the long rods resonance, their phase is reversed. This out-of-phase behavior of the long rods versus the short rods leads to destructive interference in the far-field and manifests as a quadrupolar field pattern in the near-field. This mode has a reduced net dipole moment, which in turn means negligible radiative losses.<sup>23</sup>

The diffractive and thus extended character of the SLRs can be detected by measuring the in-plane cross-polarized component (along x) of the electric near-field,  $E_x$ . Figures 4(d)–4(f) show these spectral maps for the same three frequencies as for  $E_z$ , i.e., 0.4, 0.45, and 0.5 THz. For a direct comparison, all amplitudes are normalized by the maximum absolute amplitude measured at 0.45 THz. In Fig. 4(d), we see the near-field enhancement of the  $E_x$  component around the long rod. The scattered field couples to neighboring unit cells through the (1, 0) and (−1, 0) diffractive orders. This diffraction enhanced coupling of localized resonances is the origin of the collective behavior of SLRs.<sup>41,48,49</sup>

A similar behavior as for the long rods is observed at 0.5 THz for the short rods in Fig. 4(f). However, the  $E_x$  near-field component is more complex to interpret as the long rod shows a field enhancement as well. The near-field amplitude at the transparency window, i.e., 0.45 THz, is shown in Fig. 4(e), where both rods display a strong

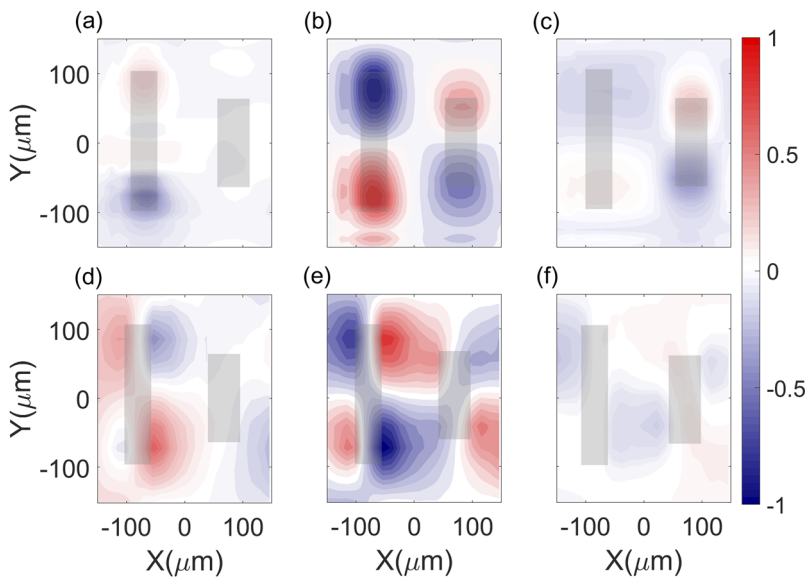


**FIG. 4.** Near-field THz amplitude maps of a single unit cell in a bare array of detuned resonators, showing the electric field enhancement: out-of-plane (or z) near-field component at (a) 0.4, (b) 0.45, and (c) 0.5 THz, and in-plane (or x) near-field component at (d) 0.4, (e) 0.45, and (f) 0.5 THz. These measurements are normalized to the maximum field intensity, which for both  $E_z$  and  $E_x$  occurs at the DET frequency of 0.45 THz, (b) and (e), respectively. The shaded gray areas indicate the location of the gold rods.

scattering of the incident radiation. Furthermore, at this frequency, the scattered fields couple with each other, across the unit cell and beyond, directly visualizing the interference between the two SLRs and the extension of the field beyond the single unit cell.

The THz amplitude maps of the array covered with graphene are shown in Figs. 5(a)–5(f). The near-fields have been recorded for the same electric field components and frequencies as for the bare array. In order to quantitatively show the effect of graphene on both  $E_z$  and  $E_x$ , all amplitudes are normalized to the maximum amplitude of the bare array of detuned resonators. From the scale bar in the figure, it is already evident that the amplitude of the near-field is significantly reduced. Figures 5(a) and 5(c) show the  $E_z$  component of the near-fields at 0.4 and 0.5 THz, respectively. The field amplitudes are both reduced by half with respect to the bare array. At 0.4 THz, we can observe near-field enhancement of both the long and short rod, in contrast to the measurements on the bare array where the enhancement was observed only near the long rod. This observation indicates that the resonances have broadened and have a response that is no longer limited to their  $\lambda/2$  natural resonant frequency.<sup>50</sup>

At the transparency window (0.45 THz), the near-field enhancement is reduced by a factor 10 at the long rod and by a factor 2 at the short rod, as can be seen in Fig. 5(b). Furthermore, the near-field amplitude also shows a depolarization field for the long rod that is created by charge carriers in the graphene layer. This depolarization field has the opposite phase with respect to the long rod, reducing its net dipole moment. This effect can be observed more clearly in the simulations shown in Fig. SI.5 in the [supplementary material](#). Figure 5(d) shows the  $E_x$  component of the near-field at 0.4 THz. The field pattern is noticeably different to the one measured for the bare array in Fig. 4(d). Both rods show a near-field enhancement in-phase with the incident field, so the scattered radiation in the plane will interfere destructively. The in-plane near-field at the transparency window, i.e., at 0.45 THz, is shown in Fig. 5(e), where the field profile looks similar to Fig. 4(e). However,

the amplitude is reduced by a factor 4, resulting in a reduction of the interference between SLRs and suppression of the transparency window. The near-field at 0.5 THz [Fig. 5(f)] is similar to that at 0.4 THz, being in-phase with the incident field. The sensitivity of the array to the presence of graphene opens the possibility to actively modulate the transparency window by changing the properties of the graphene layer, results of which will be presented in Sec. II D.

#### D. Modulation of the transparency window

The response of graphene to THz radiation can be modeled as an infinitely thin sheet with an in-plane conductivity that is governed by the carrier scattering time and the Fermi level ( $E_F$ ).<sup>51</sup> While the scattering time mainly depends on the quality of graphene,  $E_F$  can be modified by doping,<sup>52–54</sup> gating,<sup>32</sup> or by controlling the medium surrounding graphene.<sup>55</sup> The modification of  $E_F$  will exert control over the THz transparency window. As a proof of concept, we have modified the properties of graphene by annealing the sample in an argon flushed oven at 150 °C for 10 h. Annealing removes impurities adsorbed at the surface, such as water vapor, that accumulate over time by exposure to ambient conditions. The removal of these impurities decreases  $E_F$ , bringing graphene close to the Dirac point.<sup>56</sup> From the moment the sample is taken out of the oven, molecules start adsorbing onto the graphene, slowly increasing  $E_F$ . Figure 6 shows the transmittance for the sample right after annealing and two spectra after exposure to ambient conditions. These spectra are normalized to the transmittance at the DET frequency (0.45 THz) of the sample measured right after annealing the graphene.

The Fermi level was determined by comparing the far-field spectra with simulated transmittance spectra. These simulations were carried out using a Finite Difference Time Domain (FDTD) software package (Lumerical) and are shown in Fig. 6 as solid curves. For more information regarding the simulations, see Fig. SI.3 in the [supplementary material](#). The graphene layer is modeled to have a constant scattering rate of 5 meV, while varying  $E_F$  in the

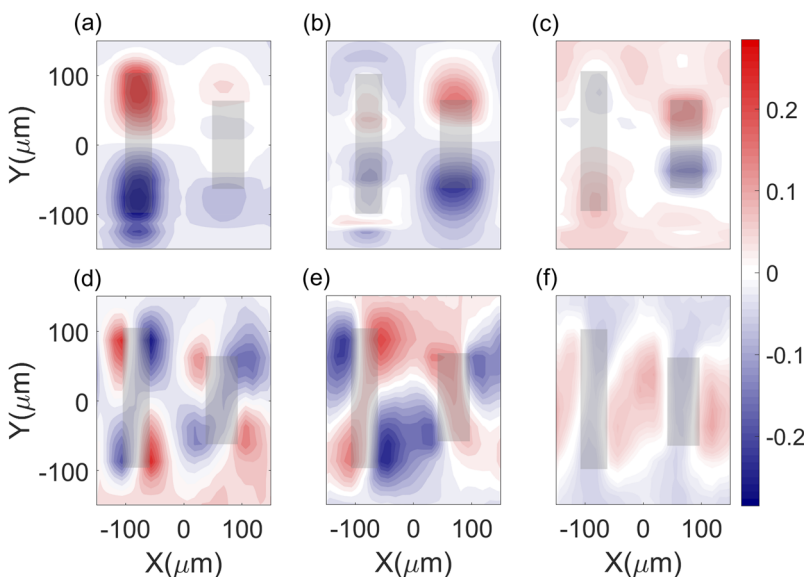


**FIG. 5.** Near-field THz amplitude maps of a single unit cell in an array of detuned resonators covered by graphene: out-of-plane (or  $z$ ) component at (a) 0.4, (b) 0.45, and (c) 0.5 THz, and near-field in-plane (or  $x$ ) component at (d) 0.4, (e) 0.45, and (f) 0.5 THz. These measurements are normalized to the same maximum values ( $z$  and  $x$  components) from Fig. 4 to highlight the suppression of the field amplitude induced by the graphene layer. The shaded gray areas indicate the location of the gold rods.

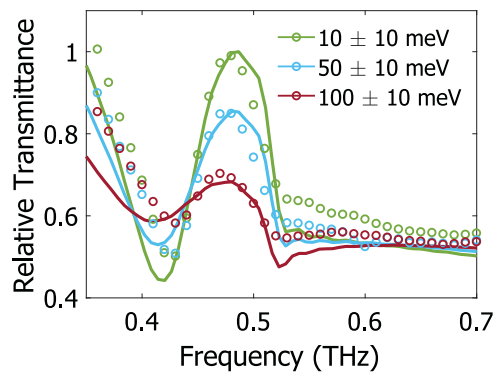


**FIG. 6.** Modulation of the relative transmittance by the array of detuned resonators covered with graphene of different  $E_F$ , showing a comparison between measured (dots) and simulated (curves) transmittance through the gold-graphene hybrid structure. The sample was first annealed in an argon atmosphere at  $150^\circ\text{C}$  resulting in an  $E_F \approx 10\text{ meV}$ . The other measurements were taken several hours after, when the adsorption of water molecules had gradually doped the graphene, increasing  $E_F$ . The transmittance at  $0.48\text{ THz}$  for  $E_F = 10\text{ meV}$  was used to normalize the spectra for an easier comparison of the results. The spectra normalized to the quartz substrate are shown in Fig. S1.3.

simulations. The three spectra shown in Fig. 6 were found to closely resemble the relative transmittance with graphene for Fermi levels of 10, 50, and 100 meV. A partial recovery of the transparency window can be observed for the annealed sample with  $E_F \approx 10\text{ meV}$ . As more ambient molecules adsorb onto graphene  $E_F$  rises, leading to more free carrier absorption and the suppression of the transparency window. This modulation of  $E_F$  provides an accurate control over DET. The addition of graphene on top of the array attenuates the field enhancement and thus quenches the DET. A simple explanation for this reduction would be the enhanced THz absorption of SLRs by the monolayer of graphene on the surface. As we show in Sec. II E, the explanation is more subtle as it involves the excitation of a metal-insulator-metal (MIM) resonance that is confined to the space between the gold rods and the graphene layer.

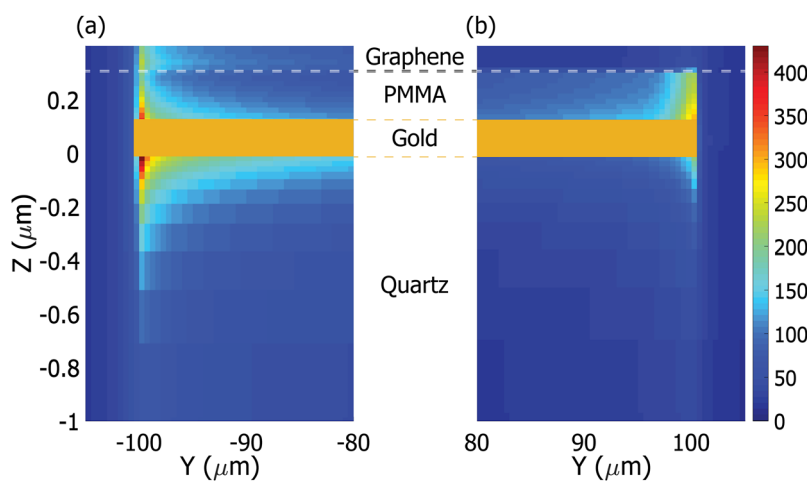


**FIG. 7.** Electric field enhancement  $|E|$  at  $0.4\text{ THz}$  normalized to the incident field, recorded in the Y-Z plane that cuts through the  $200\text{ }\mu\text{m}$  long rod of a gold-graphene metasurface. The simulation was conducted without (a) and with (b) graphene ( $E_F = 10\text{ meV}$ ) on top. A PMMA insulating layer was present in both simulations.

## E. Hybrid gap plasmons

To better understand the mechanisms leading to the reduction in DET, we have simulated the electric field distribution between the gold rods and graphene. We have analyzed the near-field distribution around the gold-graphene structure in the absence and presence of graphene, as shown in Figs. 7(a) and 7(b), respectively. These figures show a side view of the field magnitude  $|E|$  as a function of positions Y and Z simulated at the edge of the  $200\text{ }\mu\text{m}$  long rod. The simulation is performed at  $0.4\text{ THz}$ , i.e., at the frequency at which the  $\lambda/2$  resonance of the long rod dominates the near-field response. For clarity, the rod of gold and the position of the graphene layer are highlighted in Fig. 7. The field concentrates in the high index quartz substrate in the absence of graphene, forming the SLRs that give rise to DET; see Fig. 7(a). The presence of the monolayer of graphene gives rise to a very different near-field distribution: instead of the field extending in the quartz substrate, it is now confined between the gold rods and graphene.

This near-field distribution resembles that of Metal-Insulator-Metal (MIM) structures supporting gap plasmons.<sup>57</sup> These structures consist of two metal layers separated by a thin dielectric gap. A variant of MIM structures are the so-called particles on a mirror or patch antennas, in which a resonant conducting structure is placed on top of a metallic surface.<sup>58</sup> A mirror charge is generated by the metallic surface when driving the particle on resonance, which produces a very large field enhancement and confinement if the distance of the particle to the surface is small. This concept is similar to microstrip patch antennas at low frequencies using perfect conductors.<sup>59</sup> Extreme field confinement was demonstrated recently at mid-IR frequencies using gold resonant particles on a conducting graphene layer separated by a monoatomic layer of boron nitride.<sup>60</sup> In this system, the electromagnetic field is confined in the boron nitride layer by the excitation of low loss gap plasmons. In our case, a similar sample geometry is realized, consisting of a resonant metallic particle separated by a dielectric layer from a graphene sheet. The high field enhancement in this dielectric spacer suggests that the suppression of DET is due to the excitation of this gap plasmon mode. As the field is now more localized and gets absorbed by graphene, it can not propagate and interfere to generate DET, which leads to damping in the hybrid gold-graphene structure.



### III. CONCLUSION

We have investigated the formation and suppression of DET at THz frequencies in arrays of detuned resonators formed by gold rods of different dimensions by directly measuring the near-field distribution. DET originates from the interference of two SLRs in the array excited by frequency detuned rods. The fact that these SLRs are of similar amplitude but opposite in phase is responsible for the DET and manifests itself as a quadrupolar field pattern in the near-field at the transparency frequency. DET can be suppressed with a monoatomic layer of graphene on top of the array. This suppression is mediated both by absorption, as well as by the efficient excitation of gap plasmons in the hybrid metal-insulator-metal structure defined by the conducting graphene layer and the gold rods. The transmission at the transparency frequency is modified by controlling the Fermi level in the graphene layer through doping with molecular adsorption. Hybrid graphene-metal structures with properties as the ones demonstrated in this manuscript, namely, nearly full transmission at a resonance frequency, extreme field confinement in deep subwavelength layers, and active control of the THz response in a large scale device represents a very interesting metamaterial platform for the manipulation of THz radiation.

### SUPPLEMENTARY MATERIAL

In the [supplementary material](#), we have included transmittance spectra of the individual components that make up the array. A comparison is shown between the simulated and measured transmittance through the graphene covered array, to quantify the Fermi level by ambient doping. It also includes detailed simulations of the near-field distribution in a single unit cell with and without graphene on top.

### ACKNOWLEDGMENTS

We acknowledge Rochan Sinha for annealing the sample and Karsten Arts for useful discussions.

This work was funded by Nederlandse Organisatie voor Wetenschappelijk Onderzoek (NWO) (No. 680-47-628), the NWO-Philips Industrial Partnership Program NanoPhotonics for Solid State Lighting, and the European Research Council (ERC) (Nos. 259272 and 665619).

### REFERENCES

- <sup>1</sup>E. Hutter and J. H. Fendler, "Exploitation of localized surface plasmon resonance," *Adv. Mater.* **16**(19), 1685–1706 (2004).
- <sup>2</sup>S. A. Maier and H. A. Atwater, "Plasmonics: Localization and guiding of electromagnetic energy in metal/dielectric structures," *J. Appl. Phys.* **98**(1), 011101 (2005).
- <sup>3</sup>N. Yu, P. Genevet, M. A. Kats, F. Aieta, J.-P. Tetienne, F. Capasso, and Z. Gaburro, "Light propagation with phase discontinuities reflection and refraction," *Science* **334**, 333–337 (2011).
- <sup>4</sup>V. V. Popov, "Plasmon excitation and plasmonic detection of terahertz radiation in the grating-gate field-effect-transistor structures," *J. Infrared, Millimeter, Terahertz Waves* **32**(10), 1178–1191 (2011).
- <sup>5</sup>S. B. Glybovski, S. A. Tretyakov, P. A. Belov, Y. S. Kivshar, and C. R. Simovski, "Metasurfaces: From microwaves to visible," *Phys. Rep.* **634**, 1 (2016).
- <sup>6</sup>J. He and Y. Zhang, "Metasurfaces in terahertz waveband," *J. Phys. D: Appl. Phys.* **50**(46), 464004–464015 (2017).

- <sup>7</sup>A. Li, S. Singh, and D. Sievenpiper, "Metasurfaces and their applications," *Nanophotonics* **7**(6), 989–1011 (2018).
- <sup>8</sup>S. Zhang, D. A. Genov, Y. Wang, M. Liu, and X. Zhang, "Plasmon-induced transparency in metamaterials," *Phys. Rev. Lett.* **101**(4), 047401 (2008).
- <sup>9</sup>K.-J. Boller, A. Imamolu, and S. E. Harris, "Observation of electromagnetically induced transparency," *Phys. Rev. Lett.* **66**(20), 2593–2596 (1991).
- <sup>10</sup>L. Vestergaard Hau, S. E. Harris, Z. Dutton, and C. H. Behroozi, "Light speed reduction to 17 metres per second in an ultracold atomic gas," *Nature* **397**, 594–598 (1999).
- <sup>11</sup>J. Zhang, L. Cai, W. Bai, Y. Xu, and G. Song, "Slow light at terahertz frequencies in surface plasmon polariton assisted grating waveguide," *J. Appl. Phys.* **106**(10), 103715 (2009).
- <sup>12</sup>Z.-G. Dong, H. Liu, J.-X. Cao, T. Li, S.-M. Wang, S.-N. Zhu, and X. Zhang, "Enhanced sensing performance by the plasmonic analog of electromagnetically induced transparency in active metamaterials," *Appl. Phys. Lett.* **97**(11), 114101 (2010).
- <sup>13</sup>C. L. Garrido Alzar, M. A. G. Martinez, P. Nussenzeig, C. L. Garrido Alzar, M. A. G. Martinez, and P. Nussenzeig, "Classical analog of electromagnetically induced transparency," *Am. J. Phys.* **70**(1), 37–41 (2001).
- <sup>14</sup>Z. Zhu, X. Yang, J. Gu, J. Jiang, W. Yue, Z. Tian, M. Tonouchi, J. Han, and W. Zhang, "Broadband plasmon induced transparency in terahertz metamaterials," *Nanotechnology* **24**(21), 214003–214010 (2013).
- <sup>15</sup>J. Gu, R. Singh, X. Liu, X. Zhang, Y. Ma, S. Zhang, S. A. Maier, Z. Tian, A. K. Azad, H. T. Chen, A. J. Taylor, J. Han, and W. Zhang, "Active control of electromagnetically induced transparency analogue in terahertz metamaterials," *Nat. Commun.* **3**, 1151–1156 (2012).
- <sup>16</sup>N. Liu, L. Langguth, T. Weiss, J. Kästel, M. Fleischhauer, T. Pfau, and H. Giessen, "Plasmonic analogue of electromagnetically induced transparency at the Drude damping limit," *Nat. Mater.* **8**(9), 758–762 (2009).
- <sup>17</sup>P. Tassin, L. Zhang, Th. Koschny, E. N. Economou, and C. M. Soukoulis, "Low-loss metamaterials based on classical electromagnetically induced transparency," *Phys. Rev. Lett.* **102**(5), 053901 (2009).
- <sup>18</sup>S.-Y. Chiam, R. Singh, C. Rockstuhl, L. Falk, W. Zhang, and A. A. Bettiol, "Analogue of electromagnetically induced transparency in a terahertz metamaterial," *Phys. Rev. B* **80**(15), 153103 (2009).
- <sup>19</sup>S. I. Bozhevolnyi, A. B. Evlyukhin, A. Pors, M. G. Nielsen, M. Willatzen, and O. Albrektsen, "Optical transparency by detuned electrical dipoles," *New J. Phys.* **13**(2), 023034 (2011).
- <sup>20</sup>V. V. Khardikov, E. O. Iarko, and S. L. Prosvirnin, "A giant red shift and enhancement of the light confinement in a planar array of dielectric bars," *J. Opt.* **14**(3), 35103–35110 (2012).
- <sup>21</sup>M. Manjappa, Y. K. Srivastava, and R. Singh, "Lattice-induced transparency in planar metamaterials," *Phys. Rev. B* **94**(16), 161103(R) (2016).
- <sup>22</sup>A. Halpin, N. van Hoof, A. Bhattacharya, C. Mennes, and J. G. Rivas, "Terahertz diffraction enhanced transparency probed in the near field," *Phys. Rev. B* **96**(8), 085110 (2017).
- <sup>23</sup>M. C. Schaafsma, A. Bhattacharya, and J. G. Rivas, "Diffraction enhanced transparency and slow THz light in periodic arrays of detuned and displaced dipoles," *ACS Photonics* **3**(9), 1596–1603 (2016).
- <sup>24</sup>K. I. Bolotin, K. J. Sikes, Z. Jiang, M. Klima, G. Fudenberg, J. Hone, P. Kim, and H. L. Stormer, "Ultra-high electron mobility in suspended graphene," *Solid State Commun.* **146**(9–10), 351–355 (2008).
- <sup>25</sup>A. N. Grigorenko, M. Polini, and K. S. Novoselov, "Graphene plasmonics," *Nat. Photonics* **6**(11), 749–758 (2012).
- <sup>26</sup>S. V. Morozov, K. S. Novoselov, M. I. Katsnelson, F. Schedin, D. C. Elias, J. A. Jaszczak, and A. K. Geim, "Giant intrinsic carrier mobilities in graphene and its bilayer," *Phys. Rev. Lett.* **100**(1), 016602 (2008).
- <sup>27</sup>N. Sule, K. J. Willis, S. C. Hagness, and I. Knezevic, "Terahertz-frequency electronic transport in graphene," *Phys. Rev. B* **90**(4), 045431 (2014).
- <sup>28</sup>A. Yu. Nikitin, F. Guinea, F. J. García-Vidal, and L. Martín-Moreno, "Edge and waveguide terahertz surface plasmon modes in graphene microribbons," *Phys. Rev. B* **84**(16), 161407(R) (2011).
- <sup>29</sup>F. H. L. Koppens, D. E. Chang, and F. Javier García De Abajo, "Graphene plasmonics: A platform for strong light-matter interactions," *Nano Lett.* **11**(8), 3370–3377 (2011).

- <sup>30</sup>S. Thongrattanasiri, F. H. L. Koppens, and F. Javier García De Abajo, "Complete optical absorption in periodically patterned graphene," *Phys. Rev. Lett.* **108**(4), 047401 (2012).
- <sup>31</sup>J. H. Chen, C. Jang, S. Xiao, M. Ishigami, and M. S. Fuhrer, "Intrinsic and extrinsic performance limits of graphene devices on SiO<sub>2</sub>," *Nat. Nanotechnol.* **3**(4), 206–209 (2008).
- <sup>32</sup>P. Q. Liu, I. J. Luxmoore, S. A. Mikhailov, N. A. Savostianova, F. Valmorra, J. Faist, and G. R. Nash, "Highly tunable hybrid metamaterials employing splitting resonators strongly coupled to graphene surface plasmons," *Nat. Commun.* **6**, 8969 (2015).
- <sup>33</sup>M. Amin, M. Farhat, and H. Bağcı, "A dynamically reconfigurable Fano metamaterial through graphene tuning for switching and sensing applications," *Sci. Rep.* **3**, 2105 (2013).
- <sup>34</sup>Y. Zhang, Y. Feng, B. Zhu, J. Zhao, and T. Jiang, "Graphene based tunable metamaterial absorber and polarization modulation in terahertz frequency," *Opt. Express* **22**(19), 22743–22752 (2014).
- <sup>35</sup>Z. Miao, Q. Wu, X. Li, Q. He, K. Ding, Z. An, Y. Zhang, and L. Zhou, "Widely tunable terahertz phase modulation with gate-controlled graphene metasurfaces," *Phys. Rev. X* **5**(4), 041027 (2015).
- <sup>36</sup>O. Balci, N. Kakenov, E. Karademir, S. Balci, S. Cakmakyapan, E. O. Polat, H. Caglayan, E. Ozbay, and C. Kocabas, "Electrically switchable metadivices via graphene," *Sci. Adv.* **4**(1), ea01749 (2018).
- <sup>37</sup>M. Habib, A. Rahimi Rashed, E. Ozbay, and H. Caglayan, "Graphene-based tunable plasmon induced transparency in gold strips," *Opt. Mater. Express* **8**(4), 1069–1074 (2018).
- <sup>38</sup>T.-T. Kim, H.-D. Kim, R. Zhao, S. S. Oh, T. Ha, D. S. Chung, Y. H. Lee, B. Min, and S. Zhang, "Electrically tunable slow light using graphene metamaterials," *ACS Photonics* **5**, 1800–1807 (2018).
- <sup>39</sup>L. Martín-Moreno, F. J. García-Vidal, H. J. Lezec, K. M. Pellerin, T. Thio, J. B. Pendry, and T. W. Ebbesen, "Theory of extraordinary optical transmission through subwavelength hole arrays," *Phys. Rev. Lett.* **86**(6), 1114–1117 (2001).
- <sup>40</sup>F. J. García de Abajo, J. J. Sáenz, I. Campillo, and J. S. Dolado, "Site and lattice resonances in metallic hole arrays," *Opt. Express* **14**(1), 7–18 (2006).
- <sup>41</sup>B. Auguie and W. L. Barnes, "Collective resonances in gold nanoparticle arrays," *Phys. Rev. Lett.* **101**(14), 143902 (2008).
- <sup>42</sup>X. Li, W. Cai, J. An, S. Kim, J. Nah, D. Yang, R. Piner, A. Velamakanni, I. Jung, E. Tutuc, S. K. Banerjee, L. Colombo, and R. S. Ruoff, "Large-area synthesis of high-quality and uniform graphene films on copper foils," *Science* **324**(5932), 1312–1314 (2009).
- <sup>43</sup>R. H. J. Vervuurt, B. Karasulu, M. A. Verheijen, W. M. M. Kessels, and A. A. Bol, "Uniform atomic layer deposition of Al<sub>2</sub>O<sub>3</sub> on graphene by reversible hydrogen plasma functionalization," *Chem. Mater.* **29**(5), 2090–2100 (2017).
- <sup>44</sup>K. Arts, R. Vervuurt, A. Bhattacharya, J. G. Rivas, J. Willem Oosterbeek, and A. A. Bol, "Broadband optical response of graphene measured by terahertz time-domain spectroscopy and FTIR spectroscopy," *J. Appl. Phys.* **124**(7), 73105–73110 (2018).
- <sup>45</sup>C. Lee, J. Y. Kim, S. Bae, K. S. Kim, B. H. Hong, and E. J. Choi, "Optical response of large scale single layer graphene," *Appl. Phys. Lett.* **98**(7), 071905 (2011).
- <sup>46</sup>M. Wächter, M. Nagel, and H. Kurz, "Tapered photoconductive terahertz field probe tip with subwavelength spatial resolution," *Appl. Phys. Lett.* **95**(4), 041112 (2009).
- <sup>47</sup>A. Bhattacharya and J. G. Rivas, "Full vectorial mapping of the complex electric near-fields of THz resonators," *APL Photonics* **1**(8), 086103 (2016).
- <sup>48</sup>S. Zou, N. Janel, and G. C. Schatz, "Silver nanoparticle array structures that produce remarkably narrow plasmon lineshapes," *J. Chem. Phys.* **120**(23), 10871–10875 (2004).
- <sup>49</sup>V. G. Kravets, F. Schedin, and A. N. Grigorenko, "Extremely narrow plasmon resonances based on diffraction coupling of localized plasmons in arrays of metallic nanoparticles," *Phys. Rev. Lett.* **101**(8), 087403 (2008).
- <sup>50</sup>L. Novotny, "Effective wavelength scaling for optical antennas," *Phys. Rev. Lett.* **98**(26), 266802 (2007).
- <sup>51</sup>A. H. Castro Neto, F. Guinea, N. M. R. Peres, K. S. Novoselov, and A. K. Geim, "The electronic properties of graphene," *Rev. Mod. Phys.* **81**, 109 (2007).
- <sup>52</sup>A. Kasry, M. A. Kuroda, G. J. Martyna, G. S. Tulevski, and A. A. Bol, "Chemical doping of large-area stacked graphene films for use as transparent, conducting electrodes," *ACS Nano* **4**(7), 3839–3844 (2010).
- <sup>53</sup>L. D'Arسيé, S. Esconjauregui, R. S. Weatherup, X. Wu, W. E. Arter, H. Sugime, C. Cepek, and J. Robertson, "Stable, efficient p-type doping of graphene by nitric acid," *RSC Adv.* **6**(114), 113185–113192 (2016).
- <sup>54</sup>D. Liu, M. He, C. Huang, X. Sun, and B. Gao, "Fermi-level dependence of the chemical functionalization of graphene with benzoyl peroxide," *J. Phys. Chem. C* **121**(19), 10546–10551 (2017).
- <sup>55</sup>Y. Wang, Z. Ni, T. Yu, Z. X. Shen, H. Wang, Y. Wu, W. Chen, and A. T. S. Wee, "Raman studies of monolayer graphene: The substrate effect," *J. Phys. Chem. C* **112**(29), 10637–10640 (2008).
- <sup>56</sup>K. S. Novoselov, A. K. Geim, S. V. Morozov, D. Jiang, Y. Zhang, S. V. Dubonos, I. V. Grigorieva, and A. A. Firsov, "Electric field effect in atomically thin carbon films," *Science* **306**(5696), 666–669 (2004).
- <sup>57</sup>H. T. Miyazaki and Y. Kurokawa, "Squeezing visible light waves into a 3-nm-thick and 55-nm-long plasmon cavity," *Phys. Rev. Lett.* **96**(9), 097401 (2006).
- <sup>58</sup>R. Esteban, T. V. Teperik, and J. J. Greffet, "Optical patch antennas for single photon emission using surface plasmon resonances," *Phys. Rev. Lett.* **104**(2), 026802 (2010).
- <sup>59</sup>Y. Zhang, J. Von Hagen, M. Younis, C. Fischer, and W. Wiesbeck, "Planar artificial magnetic conductors and patch antennas," *IEEE Trans. Antennas Propag.* **51**(10), 2704–2712 (2003).
- <sup>60</sup>D. Alcaraz Iranzo, S. Nanot, E. J. C. Dias, I. Epstein, C. Peng, D. K. Efetov, M. B. Lundeberg, R. Parret, J. Osmond, J. Yong Hong, J. Kong, D. R. Englund, N. M. R. Peres, and F. H. L. Koppens, "Probing the ultimate plasmon confinement limits with a van der Waals heterostructure," *Science* **360**(6386), 291–295 (2018).